## Title

Time-resolved SWIR imaging for the assessment of the activity of occlusal caries lesions



## Journal

Journal of Biophotonics, 16(10)

## ISSN

1864-063X

## Authors

Ng, Morgan
Wycoff, Spencer
Zhu, Yihua
et al.

## Publication Date

2023-10-01

## DOI

10.1002/jbio.202300165

Peer reviewed

HHS Public Access

Author manuscript

*J Biophotonics*. Author manuscript; available in PMC 2024 October 01.

Published in final edited form as:

*J Biophotonics*. 2023 October ; 16(10): e202300165. doi:10.1002/jbio.202300165.

# Time-resolved SWIR imaging for the assessment of the activity of occlusal caries lesions

**Morgan Ng**[1], **Spencer Wycoff**[1], **Yihua Zhu**[1], **Yi-Ching Ho**[1,2], **Hannah Takasuka**[1], **Daniel Fried**[1,*]

[1]University of California, San Francisco, San Francisco, California 94143-0758

[2]Department of Stomatology, Taipei Veterans General Hospital, Taipei, Taiwan 11217

## Abstract

The aim of this study was to develop a clinical SWIR reflectance handpiece to assess the activity of lesions on the occlusal surfaces. The time-resolved reflectivity of ten active and ten arrested occlusal caries lesions on extracted teeth was monitored at 1470 nm using a benchtop system and a modified clinical prototype during forced air drying. The presence of a highly mineralized surface zone measured with microcomputed tomography (microCT) was used to indicate lesion activity. Multiple kinetic parameters were extracted from the acquired SWIR time versus intensity dehydration curves and used to assess lesion activity. Three parameters: delay, $\%I_{fin}$, and rate calculated from the SWIR dehydration curves were significantly different ($P < 0.05$) between active and arrested lesions. The modified clinical probe was able to completely dehydrate all the active lesion areas in the occlusal pits and fissures in less than 30 seconds.

## Graphical Abstract

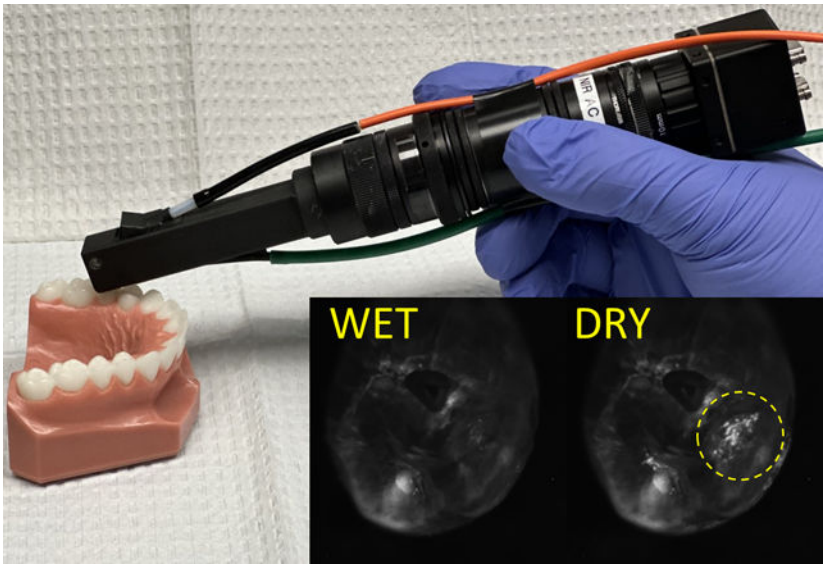


*Corresponding Author Daniel.fried@ucsf.edu.

Many caries lesions (tooth decay) are arrested and do not need intervention. A clinical SWIR reflectance handpiece was developed that can be used to assess lesion activity. The handpiece operating at 1470 nm was able to differentiate active from arrested occlusal caries lesions on twenty extracted teeth.

**Keywords**

dental caries; SWIR imaging; lesion activity; occlusal lesions; lesion activity

## 1. Introduction

Caries lesions can be arrested by the preferential deposition of mineral at the lesion surface that inhibits diffusion of fluids [1–4]. Since arrested lesions do not need further intervention, the assessment of lesion activity is essential for clinical diagnosis. Conventional visual and tactile methods of lesion activity assessment are not reliable [5]. Gold standards for lesion assessment such as transverse microradiography (TMR) and polarized light microscopy (PLM) either require destruction of the tooth, or in the case of microcomputed tomography (microCT) are not suitable for use *in-vivo*. Non-destructive diagnostic tools are needed that can assess lesion activity in a single visit. New optical diagnostic technologies that can monitor optical changes in the light scattering of lesion structures have great potential for assessing activity. Optical coherence tomography (OCT) can be used to assess lesion activity in a single measurement nondestructively in vivo; however such systems are expensive and there are no systems currently available for clinical use. OCT is capable of detecting the presence of a highly mineralized surface zone near the lesion surface which appears as a transparent surface zone due to the reduced reflectivity [4, 6, 7]. Short wavelength infrared (SWIR) imaging offers a novel and complementary approach that exploit changes in light scattering and absorption that occur in the lesion during the loss of water from the lesion structure [8, 9].

When lesions become arrested by mineral deposition, or remineralization of the outer layers of the lesion, the diffusion of fluids into the lesion are inhibited. Hence, the rate of water diffusion out of the lesion or the evaporation kinetics or dynamics reflects the degree of lesion activity. Since arrested lesions are less permeable to water due to the highly mineralized surface layer, changes in the rate of water loss can be related to changes in lesion structure and porosity. Changes in fluorescence loss [10–12], thermal emission, and SWIR reflectance [8, 9, 13–17] during lesion dehydration have been investigated as methods for assessing lesion activity. Sound enamel is transparent at SWIR wavelengths, whereas early demineralization causes increased SWIR reflectance due to scattering [18]. Water in the pores at the surface of the lesion absorbs the incident SWIR light, particularly at wavelengths greater than 1400 nm, reducing surface scattering and lesion contrast [19, 20]. Loss of that water due to evaporation produces a marked increase in reflectivity and lesion contrast. *In-vivo* studies have been published utilizing the fluorescence loss of white spot lesions on coronal surfaces [12] and thermal imaging to assess root caries during dehydration [21]. There is a negative association between the surface zone thickness and lesion permeability; a small increase in the surface layer thickness of less than 20 μm

can lead to a marked decrease in permeability [22]. In addition, in a closely related study the surface zone was removed from arrested lesions producing a corresponding rise in the permeability providing further confirmation of the role of the surface zone in arresting lesions [23]. Recent studies have shown that the water absorption bands at 1450 and 1950 nm are advantageous for SWIR reflectance dehydration measurements and produce higher contrast between sound and demineralized enamel [24, 25].

The first clinical study to utilize SWIR reflectance dehydration measurements was recently carried out on the occlusal surfaces of primary teeth using a compact InGaAs camera and 1400–1750 nm light [26]. The presence of a highly mineralized transparent surface zone was also assessed using cross polarization optical coherence tomography (CP-OCT). The SWIR imaging results were promising showing that the delay between the application of the forced air and the rise in reflectivity is a good indicator of lesion activity. However, there was difficulty fully dehydrating the lesions in the pits and fissures and acquiring curves suitable for complete analysis of the dehydration kinetics. That study indicated that additional work is needed to improve the acquisition of dehydration curves *in vivo* and further develop methods for analysis of dehydration curves acquired from the pits and fissures of the occlusal surfaces. In this study, we choose to use the 1450 nm water absorption band for imaging as opposed to the 1950 nm water absorption band because compact extended range InGaAs cameras suitable for clinical use operating beyond 1750 nm are not yet available and our goal was to assess the performance of a handheld system that can be used clinically at this time.

Multiple parameters describing the shape of the curves representing the rate of intensity change during dehydration can be derived from these curves including delay, $\% \Delta I$, $\% I_{fin}$, and rate [25]. Delay represents the initial delay between the time air is applied and the rise in intensity, %ΔI is the percent change in intensity before and after dehydration, $\% \Delta I = I_t/I_{t0} \times 100$ where t is the time of dehydration, the rate represents the shape of the rise in intensity and once the rise begins that typically takes a sigmoidal shape for active lesions, and $\% I_{fin}$ represents the fraction of the intensity rise that occurs after the most rapid change in intensity. For active lesions there is typically an initial delay before the rise in intensity occurs because the water in the pores near the lesion surface absorb the incident SWIR light. The curves for active lesions experience a rapid/steep rise in intensity (high rate) to quickly plateau in intensity (low $\% I_{fin}$) since the water in the body of the lesion can more rapidly escape through the open pores. For arrested lesions there is a minimal delay since the highly mineralized surface layer lacks porosity and water. Dehydration occurs slowly (low rate) because the highly mineralized surface layer blocks the pores in the lesion and inhibits the loss of water and much of the intensity change occurs slowly in the tail of the curve (high $\% I_{fin}$). The rate of increase in intensity was assessed using the Hill equation that was developed to assess ligand binding in biochemistry [27]. Previous studies used the sigmoid function to calculate an overall growth rate (OGR) calculated from two coefficients [8, 9] but we found that better fits could be achieved using the Hill equation. Both functions were designed to fit sigmoidal shaped curves. The Hill equation is given by equation 1.

$$I(t) = base + \frac{(max - base)}{1 + \left(\frac{t_{0.5}}{t}\right)^{rate}} \quad (1)$$

Where base is the intensity at time zero, max is the intensity at the maximum time (60 seconds in this study) and $t_{0.5}$ is the time at which the intensity is at (base + max)/2. The rate is determined from the best fit curve to the dehydration curves.

The fraction of the intensity change that takes place in the tail end of the curve after the initial rapid rise in reflectivity % $I_{fin}$) was calculated using equation 2.

$$\%I_{fin} = \left(\frac{I_{tend} - I_{tmax+10}}{I_{tend} - I_{to}}\right) x100 \quad (2)$$

Where $I_{to}$ and $I_{tend}$ are the intensities at the beginning and end of the curves. The time of maximum change ($t_{max}$) was calculated by taking the derivative of the dehydration curve (dI/dt) and identifying the position of maximum change.

The purpose of this study was to develop and test a more effective clinical SWIR dehydration probe for use on occlusal surfaces and develop improved methods for analysis of the acquired dehydration curves that most effectively differentiate active from arrested lesions.

## 2. Materials and Methods

### 2.1 Tooth Samples and MicroCT

Teeth were collected from patients in the San Francisco Bay area with approval from the UCSF Committee on Human Research. The teeth were sterilized using gamma radiation and stored in 0.1% thymol solution to maintain tissue hydration and prevent bacterial growth.

The teeth were imaged using Microcomputed X-ray tomography (microCT) with a 10 μm resolution. A Scanco microCT 50 from Scanco USA (Wayne, PA) was used to acquire the images. MicroCT images of 120 teeth were examined and ten teeth with occlusal lesions chosen with distinct surface zones of mineral content approaching that off sound enamel were selected and designated as arrested while ten teeth were chosen for which the surface zones were not highly mineralized and those were designated as active lesions. Often lesions are present on the tooth that are only partially arrested and have both active and arrested areas [9].

### 2.2 Visible/Color Images

A USB microscope, Model 5MP Edge AM7915MZT, AnMO Electronics Corp. (New Taipei City, Taiwan) equipped with a visible polarizer was use used to acquired visible

images of all samples. The digital microscope captures 5 mega-pixel (2952 × 1944) color images. Eight white LED lights contained in the camera illuminate the sample and a single polarization element is utilized to reduce glare.

### 2.3 SWIR Dehydration Probe Development (Handpiece)

The reflectance probe was designed in Fusion 360 from Autodesk (San Francisco, CA) and 3D printed using a Form 3 printer from Formlabs (Boston, MA). The reflectance probe body was printed using biocompatible and autoclavable Formlabs Biomed black resin. The probe is approximately 8 cm long and 14 mm in diameter at the distal end. Attached to the probe is a right-angle aluminum mirror to collect light from the occlusal surface and an assembly for the attachment of the reflectance fiber. SWIR light is delivered through a 0.4-mm diameter low-OH optical fiber from a 1466 nm superluminescent laser diode (SLD), from EXALOS (Zurich, Switzerland) with an output of 14 mW and a bandwidth of 40 nm. The fiber is inserted into a cylindrical Teflon plug (3.2×40 mm). Light exiting the plug is directed toward the tooth occlusal surface by a 5 mm polarizing beamsplitter cube. The probe employs cross-polarization to reduce specular reflection. There is an 1/8 inch air nozzle attached to the reflectance body and air exits the air channel near the mirror to prevent the fogging of the mirror and dehydrate the lesion surface to assess lesion activity [8, 9, 17]. In existing probes, the air dehydration channels are directed parallel to the probe surface (Fig. 1B). This nozzle design has worked well on tooth root surfaces [21], however dehydration in the pits and fissures of tooth occlusal surfaces has been more difficult [26]. We experimented with new preliminary nozzle designs and found that the dehydration rate can be increased markedly for occlusal surfaces by narrowing the nozzle opening and angling the nozzle. The new design is shown in Fig. 1A next to the old design along with a dehydration curve acquired from a deep fissure with an active lesion using the new nozzle prototype. In the old design (Fig. 1B) the exit ports were each 8 × 0.7 mm and oriented parallel to the long axis of the probe. In the new design (Fig. 1A), the top slit is 2 × 1.4 mm and oriented parallel to the long axis of the probe while the lower exit port is 2 × 0.75 mm and angled by 38° to the long axis.

The reflectance probe was attached to a 640 × 480 pixel micro-SWIR camera (SU640CSX) measuring only 32 × 32 × 28 mm from Sensors Unlimited (Princeton, NJ). Two planoconvex antireflection coated lenses of 60 and 100 mm focal length along with an adjustable aperture were placed between the handpiece and the InGaAs camera to provide a field of view of 11 $mm^2$ at the focus plane. A computer-controlled air nozzle with a 1 mm aperture and an air pressure set to 25 psi was connected to the probe body for dehydration. The handpiece shown in Fig. 2B was held in a clamp with the probe positioned above the occlusal surface of each tooth that was held in a vertical position in a similar configuration that would be used clinically. The efficacy of drying tooth occlusal surfaces with the new probe design was evaluated by measuring the change in intensity in a fixed 25 × 25 pixel area for 6 lesions on 6 teeth, 3 active and 3 arrested after 30 seconds of drying, where $\Delta I_{drying} = (I_0 - I_{30})/I_0$ and $I_0$ and $I_{30}$ are the intensities at 0 and 30 seconds after applying the air.

### 2.4 SWIR Dehydration Measurements

Time-resolved SWIR images were acquired of the 20 teeth using a benchtop system (Fig. 2A) and the handpiece (Fig. 2A) during drying for 60 seconds at 25 psi. The benchtop SWIR reflectance images were captured using a Model SU320KTSX (Sensors Unlimited, Princeton, NK) InGaAs camera with a 320 × 256 pixel format, a 25 μm pixel pitch and a bit depth of 12 bit. A Navitar f=35 mm / F1.4 lens was used in combination with a 1 in diameter f=75 mm planoconvex lens along with an adjustable aperture. The same 1470 nm SLD was used as a light source. SWIR polarizers were placed before the light source and camera for cross polarization imaging. Samples were stored in a moist environment to preserve internal hydration and the samples were immersed in a water bath before mounting and performing measurements. A computer-controlled air nozzle with a 1 mm aperture and an air pressure set to 25 psi was positioned 3 cm away at a 20° angle above the sample plane as shown in Fig. 2A. For the benchtop system the tooth was held in a horizontal position and for the handpiece the tooth was held in a vertical position.

After each sample was removed from the water bath, an image was captured as an initial reference image and the pressurized air nozzle was activated to dehydrate the sample. Each measurement consisted of capturing a sequence of images at 1 frame per second for 60 seconds. For each measurement, the air nozzle and the light source were centered on the region of interest (ROI) that encompasses the entire sample. The dehydration setup was completely automated using LabVIEW software from National Instruments (Austin, TX).

A custom program written using MATLAB from Mathworks (Natick, MA) was used to calculate DEL, $\% \Delta I$, rate and $\% I_{fin}$ from each curve. The first second of each acquisition was removed from each curve because large fluctuations in intensity occur due to the removal of water droplets on the tooth surface by the air. Differences between the four parameters ΔI, DEL, rate and $\% I_{fin}$ between the active and arrested groups were compared using unpaired two-tailed t-tests. Prism statistical software from GraphPad Software, Inc., (La Jolla, CA) was used for the calculations. Significance level was set at $p < 0.05$.

## 3. Results

An example of acquired intensity vs time curves using the new probe for sound and lesion areas is shown in Fig. 1F. The active lesion is located in a very deep narrow fissure as can be seen in the microCT images shown in Figs. 1C&D. Even though the fissure is very deep the new probe was effective in dehydrating the active lesion within 20–30 seconds. There was an initial delay of 7 seconds before the rapid sigmoidal rise in intensity that is typical of active lesions. The magnitude of $\Delta I_{drying}$ for the new probe vs the old reflectance probe for the 6 active and arrested lesions was more than 100 times higher.

Examples of images before and after drying acquired with the benchtop and handpiece systems are shown Figs. 3 & 4. In Fig. 3 an active lesion in a pit is shown. The color image in Fig. 3A indicates that the lesion is only slightly pigmented. The microCT image in Fig. 3B shows a narrow lesion only halfway through the enamel. The line profile of density vs position extracted at the position of the yellow line shows a surface zone of higher mineral content at the position of the red arrow with a mineral density that peaks at less than 2.5

g/cm$^3$ and is not highly mineralized. The mineral density at the position of the green arrow appears sound and approaches 3.0 g/cm$^3$. SWIR images acquired before and after drying are shown in Figs. 3C–F. The lesion area shows a dramatic change in intensity before and after drying for both the benchtop system and the handpiece.

Figure 4 shows an arrested lesion located in a fissure. The color image in Fig. 4A shows that the lesion area is highly pigmented and appears much darker than the surrounding tooth structure. The microCT image in Fig. 4B shows a fairly large lesion that penetrates to the underlying dentin. There is a highly mineralized surface zone that is much lighter than the lesion body and appears as light as the surrounding sound enamel. The line profile of density vs position extracted at the position of the yellow line shows that the mineral content of the surface zone located at the position of the red arrow approaches that of sound enamel (3.0 g/cm$^3$).

Intensity vs. time curves for the two lesions shown in Figs. 3 & 4 are plotted in Fig. 5 for both the benchtop and handpiece systems. The active lesion exhibits a measurable delay before the rapid sigmoidal rise in intensity that reaches the maximum intensity in only 12 seconds for the benchtop system and is even faster for the handpiece where it takes about 8 seconds to peak. In contrast the arrested lesion exhibits no discernable delay. The intensity slowly rises and does not achieve peak intensity after 60 seconds. Mean ± sd of delay, %ΔI, $\%I_{fin}$, and rate after 60 seconds of drying for the active (n=10) and arrested (n=10) lesion areas are tabulated in Table I for both the benchtop and handpiece systems. The significance level calculated from unpaired two-tailed t-tests between the active and arrested groups for each system is also listed. The means of delay, $\%I_{fin}$, and rate were significantly different between active and arrested lesions for both the benchtop system and the handpiece. Active lesions had a significantly higher mean ΔI% than arrested lesions for the benchtop system while there was no significant difference between the two groups with the handpiece. 3D scatterplots of delay, $\%I_{fin}$, and rate for the active lesions (red) and arrested lesions (blue) are shown in Fig. 6 for the benchtop and handpiece systems. There is clear separation in grouping in the 3D plots between the active and arrested lesions for both systems.

Differentials in the magnitude of the means between active and arrested lesions for delay, $\%I_{fin}$, and rate all exceeded ratios of 5 to 1 with rate being the highest at 9 to 1.

## 4. Discussion

Most newly discovered caries lesions are in the pits and fissures of occlusal surfaces. Such surfaces are more challenging for lesion activity assessment using time-resolved SWIR reflectance imaging due to the highly convoluted topography. In the first clinical study to assess lesion activity in vivo using time-resolved SWIR reflectance imaging, lesions located on the occlusal surfaces of primary teeth were chosen to ensure that most of the lesions would be active [26]. The study showed the potential of using the delay to discriminate between active and arrested lesions however there was considerable difficulty in sufficiently dehydrating lesions in these areas in 30 seconds. In addition, many of the acquired curves were noisy or incomplete preventing the calculation of kinetic information from the curves such as rates or $\%I_{fin}$ [26]. Values for %ΔI were calculated, however there was no significant

difference in %ΔI between active and arrested lesions. In this study and in a recent *in vitro* study [25], %ΔI was not significantly higher for active lesions compared to arrested lesions. In earlier studies that utilized simulated lesions or lesions that were confined to the outer half of enamel, %ΔI was significantly higher for active lesions [8, 9]. In those early studies, optical coherence tomography was used to assess lesion severity with deeper lesions being avoided due to the limited penetration depth of OCT. However, for this study and a recent study [25], microCT was used to image the proximal and occlusal lesions many of which were of greater severity.

The newly designed probe for the clinical handpiece with the angled and focused air nozzle was as effective as the benchtop system that had the air nozzle pointed almost directly at the tooth occlusal surfaces. A higher air pressure of 25 psi was used instead of the 10–15 psi that was used in previous studies, however this is still markedly lower than the pressures used by dental air syringes that can be as high as 80 psi. Complete dehydration of active lesions should occur within 30 seconds for practical clinical implementation. This was achieved for all the active lesions using both the benchtop system and the handpiece within 30 seconds. In contrast, complete dehydration can take hundreds of seconds for arrested lesions, however the entire curve is not needed to calculate suitable values of $\%I_{fin}$ and rate as they are sufficiently different from active lesions due to the much slower rate of dehydration for arrested lesions. Dehydration devices using the probe with the air flow shown in Fig. 1A were used in two clinical studies; one on root surfaces [21] and the second on the occlusal surfaces of primary teeth [26]. In both studies the test subjects did not complain about any pain or air sensitivity at delivery pressures of 10–15 psi. Since patients most often complain about sensitivity on root surfaces we do not anticipate any problems when using the probe on tooth coronal surfaces at higher pressures or with the more focused flow for the probe design of Fig. 1B. However, there may be issues with sensitivity if we use the more focused probe of Fig. 1B or higher air pressures on root surfaces.

Based on this study and recent studies [25, 26], it appears that %ΔI is not a reliable parameter to discriminate between active and arrested lesions and is not suitable for *in vivo* measurements since the depth and severity of the lesions is not known ahead of time. The other three parameters that reflect the kinetics of the dehydration process; delay, $\%I_{fin}$, and rate are less dependent on the lesion depth and severity and are better suited for clinical use.

A previous *in vitro* study showed that 1950 nm was best suited for lesion activity assessment using time-resolved reflectance imaging [25], however compact SWIR cameras small enough for clinical use are limited to wavelengths less than 1700 nm, thus we chose to use an SLD operating at 1470 nm which overlaps the water absorption band centered at 1450 nm.

In this study, we choose to use the Hill equation to model the kinetics of dehydration as opposed to the sigmoid function that was used previously [8, 9]. Both functions are frequently used to fit sigmoidal shaped curves, however the Hill equation performed better for many of the arrested curves for which the sigmoidal shape was not as well developed, such as the arrested curve in Fig. 5. 3D scatter plots for both the benchtop system and the handpiece using delay, $\%I_{fin}$, and rate show that the two groups are well separated for

clear discrimination between active and arrested lesions. Clinical assessments are more challenging, and it is valuable to have multiple parameters available for use. The calculation of delay, $\%I_{fin}$, and rate can be easily automated for rapid calculation and 2D projection maps can be created for those parameters in a similar fashion to what has been done previously for optical coherence tomography [6, 28].

## 5. Conclusions

In summary, this study has shown that the efficiency of dehydration can be greatly improved by modifying the air-nozzle characteristics of an existing handpiece used for time-resolved SWIR imaging and that the handpiece can perform nearly as well as a benchtop system. Complete dehydration was achieved for the ten active occlusal lesions in the study in less than 30 seconds indicating that the handpiece is practical for clinical use. Delay, $\%I_{fin}$, and rate were extracted from the acquired intensity vs time curves. Each of these parameters varied markedly between active and arrested lesions and was suitable for the assessment of lesion activity. We plan to further assess the clinical performance of the newly designed handpiece in future clinical studies.

## Acknowledgements

The authors would like to acknowledge the support of NIDCR/NIH grants R01-DE028295. The authors would like to thank Nick Chang, John Tressel, William Fried and Cynthia Darling for their contribution to this work.

## 7. References

[1]. Fejerskov O, Nyvad B, Kidd E, Dental Caries: The Disease and its Clinical Management, Wiley Blackwell, 2015.

[2]. ten Cate JM, Arends J, Remineralization of artificial enamel lesions in vitro, Caries Res 11(5) (1977) 277–86. [PubMed: 18285]

[3]. Kidd EA, The histopathology of enamel caries in young and old permanent teeth, British Dent J 155(6) (1983) 196–8.

[4]. Chan KH, Tom H, Lee RC, Kang H, Simon JC, Staninec M, Darling CL, Pelzner RB, Fried D, Clinical monitoring of smooth surface enamel lesions using CP-OCT during nonsurgical intervention, Lasers Surg Med 48(10) (2016) 915–923. [PubMed: 26955902]

[5]. Ekstrand KR, Zero DT, Martignon S, Pitts NB, Lesion activity assessment, Monographs in Oral Science 21 (2009) 63–90. [PubMed: 19494676]

[6]. Lee RC, Kang H, Darling CL, Fried D, Automated assessment of the remineralization of artificial enamel lesions with polarization-sensitive optical coherence tomography, Biomed Opt Express 5(9) (2014) 2950–62. [PubMed: 25401009]

[7]. Jones RS, Fried D, Remineralization of enamel caries can decrease optical reflectivity, J Dent Res 85(9) (2006) 804–8. [PubMed: 16931861]

[8]. Lee RC, Darling CL, Fried D, Assessment of remineralization via measurement of dehydration rates with thermal and near-IR reflectance imaging, J Dent 43 (2015) 1032–1042. [PubMed: 25862275]

[9]. Lee RC, Staninec M, Le O, Fried D, Infrared methods for assessment of the activity of natural enamel caries lesions, IEEE J Selected Top Quant Electronics 22(3) (2014) 6803609.

[10]. Stookey GK, Quantitative light fluorescence: a technology for early monitoring of the caries process, Dent Clin North Am 49(4) (2005) 753–70. [PubMed: 16150315]

[11]. Ando M, Stookey GK, Zero DT, Ability of quantitative light-induced fluorescence (QLF) to assess the activity of white spot lesions during dehydration, Am J Dent 19(1) (2006) 15–8. [PubMed: 16555651]

[12]. Ando M, Ferreira-Zandona AG, Eckert GJ, Zero DT, Stookey GK, Pilot clinical study to assess caries lesion activity using quantitative light-induced fluorescence during dehydration, J Biomed Opt 22(3) (2017) 35005. [PubMed: 28280839]

[13]. Kaneko K, Matsuyama K, Nakashima S, Quantification of Early Carious Enamel Lesions by using an Infrared Camera, in: Stookey GK (Ed.) Early detection of Dental caries II, Indiana University, Indianapolis, IN, 1999, pp. 83–99.

[14]. Zakian CM, Taylor AM, Ellwood RP, Pretty IA, Occlusal caries detection by using thermal imaging, J Dent 38(10) (2010) 788–795. [PubMed: 20599464]

[15]. Usenik P, Burmen M, Fidler A, Pernus F, Likar B, Near-infrared hyperspectral imaging of water evaporation dynamics for early detection of incipient caries, J Dent 42(10) (2014) 1242–7. [PubMed: 25150104]

[16]. Lee RC, Lee D, Darling CL, Fried D, Nondestructive assessment of the severity of occlusal caries lesions with near-infrared imaging at 1310 nm, J Biomed Optics 15(4) (2010) 047011.

[17]. Lee RC, Darling CL, Fried D, Activity assessment of root caries lesions with thermal and near-infrared imaging methods, J Biophotonics 10(3) (2016) 433–445. [PubMed: 27060450]

[18]. Darling CL, Huynh GD, Fried D, Light Scattering Properties of Natural and Artificially Demineralized Dental Enamel at 1310-nm, J Biomed Optics 11(3) (2006) 034023.

[19]. Chung S, Fried D, Staninec M, Darling CL, Multispectral near-IR reflectance and transillumination imaging of teeth Biomed Opt Express 2(10) (2011) 2804–2814. [PubMed: 22025986]

[20]. Simon JC, Chan KH, Darling CL, Fried D, Multispectral near-IR reflectance imaging of simulated early occlusal lesions: variation of lesion contrast with lesion depth and severity, Lasers Surg Med 46(3) (2014) 203–15. [PubMed: 24375543]

[21]. Yang V, Zhu Y, Curtis D, O Le N Chang, W. Fried, JC Simon, P. Banan, C. Darling, D. Fried, Thermal Imaging of Root Caries In Vivo, J Dent Res 99(13) (2020) 1502–1508. [PubMed: 32866422]

[22]. Chang NN, Jew JM, Fried D, Lesion dehydration rate changes with the surface layer thickness during enamel remineralization, Lasers in Dentistry XXIV, 2018, Proc. SPIE Vol. 10473 pp. 0D:1–7.

[23]. Liu H, Chang NY, Gao W, Fried D, Infrared imaging confirms the role of the transparent surface zone in arresting dental caries, Photonic Therapeutics and Diagnostics in Dentistry, Head and Neck Surgery, and Otolaryngology, 2021, Proc. SPIE Vol. 11627 pp. 0O:1–10.

[24]. Fried WA, Abdellaziz M, Darling CL, Fried D, High Contrast Reflectance Imaging of Enamel Demineralization and Remineralization at 1950-nm for the Assessment of Lesion Activity, Lasers Surg Med 53(7) (2020) 968–977.

[25]. Tressel J, Abdelaziz M, Fried D, Dynamic SWIR Imaging near the 1950 nm water absorption band for caries lesion diagnosis J Biomedical Opt 26(5) (2021) 056006.

[26]. Zhu Y, Kim J, Lin B Fried D, Monitoring Lesion Activity on Primary Teeth with CP-OCT and SWIR Reflectance Imaging Lasers Surg Med Early View: 10.1002/lsm.23677 (2023).

[27]. Hill AV, The possible effects of the aggregation of the molecules of haemoglobin on its dissociation curves, J Phyiol 40 (1910) 4–7.

[28]. Le MH, Darling CL, Fried D, Automated analysis of lesion depth and integrated reflectivity in PS-OCT scans of tooth demineralization, Lasers Surg Med 42(1) (2010) 62–8. [PubMed: 20077486]

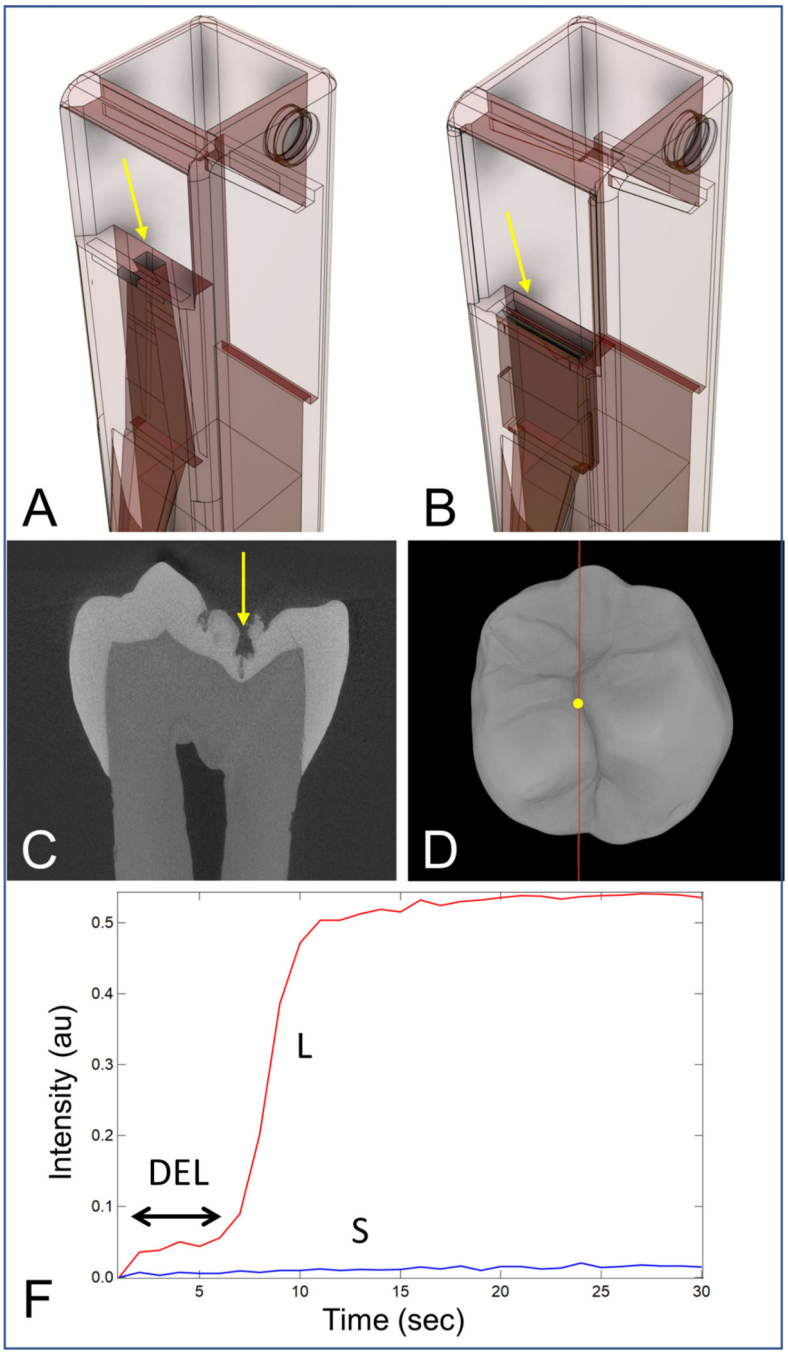


**Fig. 1.**

(A) New nozzle design showing narrow angled port (yellow arrow) and (B) old nozzle design with broad flat port. Acquired dehydration curves at 1450 nm (F) from the lesion (L) located at the position of the yellow arrow and dot in microCT images (C & D) along with a sound (S) area.

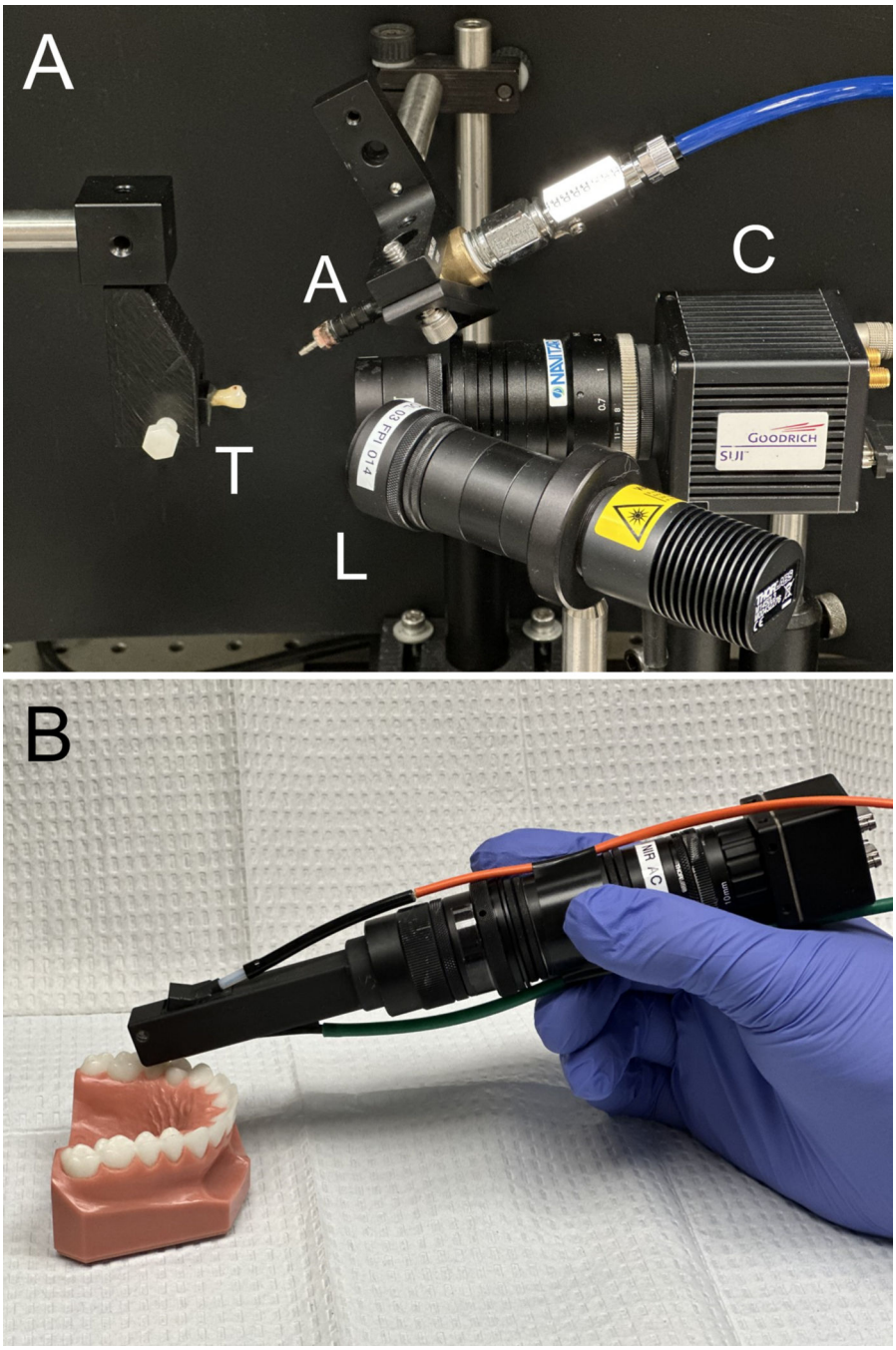


**Fig. 2.**

(A) Schematic of the experimental benchtop setup showing the tooth (T), air nozzle (A), SWIR camera (C), and 1466 nm SLED light source (L). (B) SWIR reflectance imaging handpiece with miniature SWIR camera with attached light delivery fiber (orange) and air line (green).

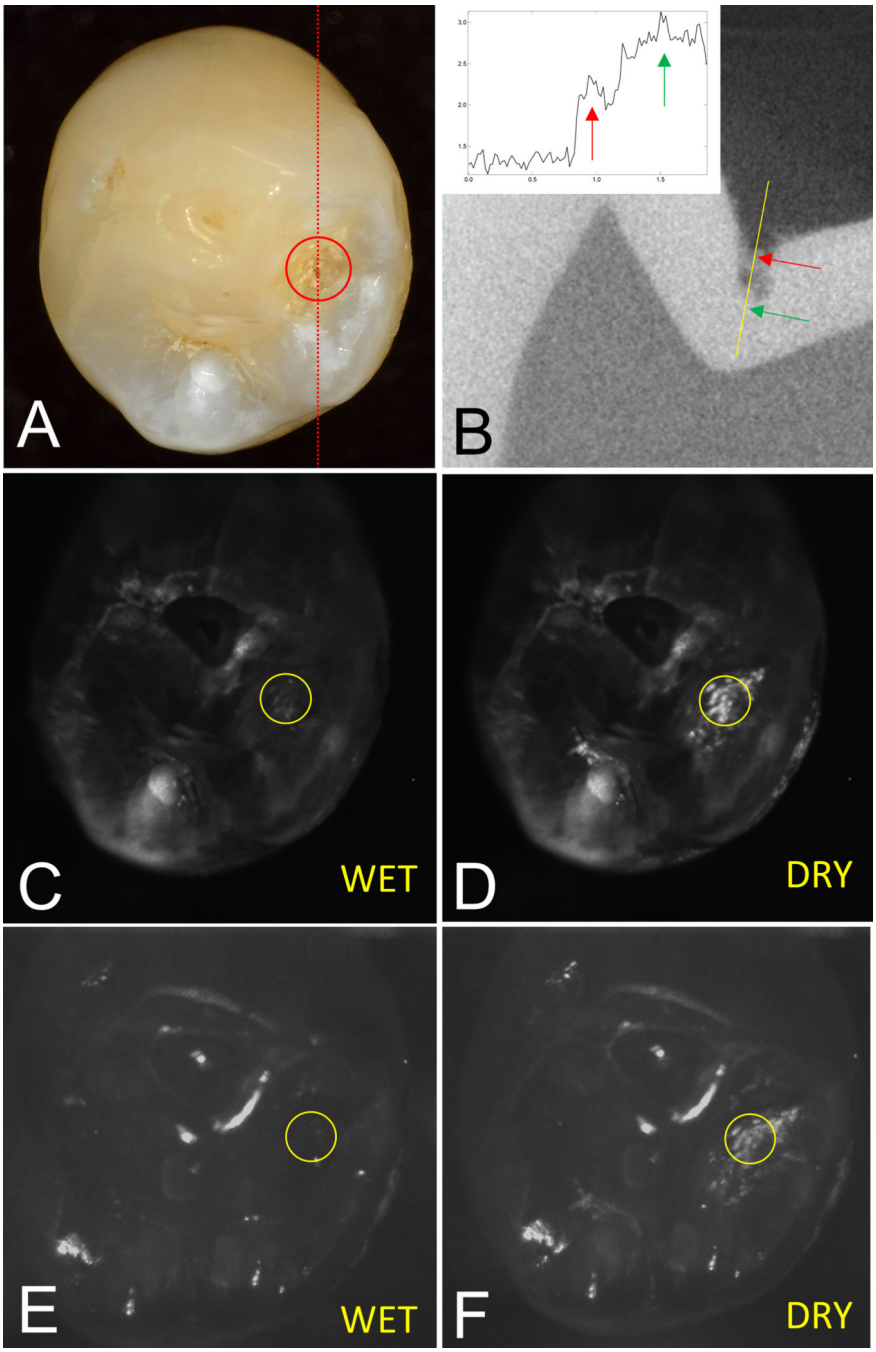


**Fig. 3.**

(A) Color image of a tooth with an active lesion (red circle). (B) MicroCT image showing the lesion and inset shows a line profile of the mineral density vs position extracted at the position of the yellow line. Red arrow shows the position of the lesion surface zone while the green arrow shows the position of the underlying sound enamel in the extracted line profile. SWIR images acquired with the (C&D) benchtop system and handpiece (E&F) before (wet) and after (dry) drying the lesion for seconds. Yellow circle is the lesion area.

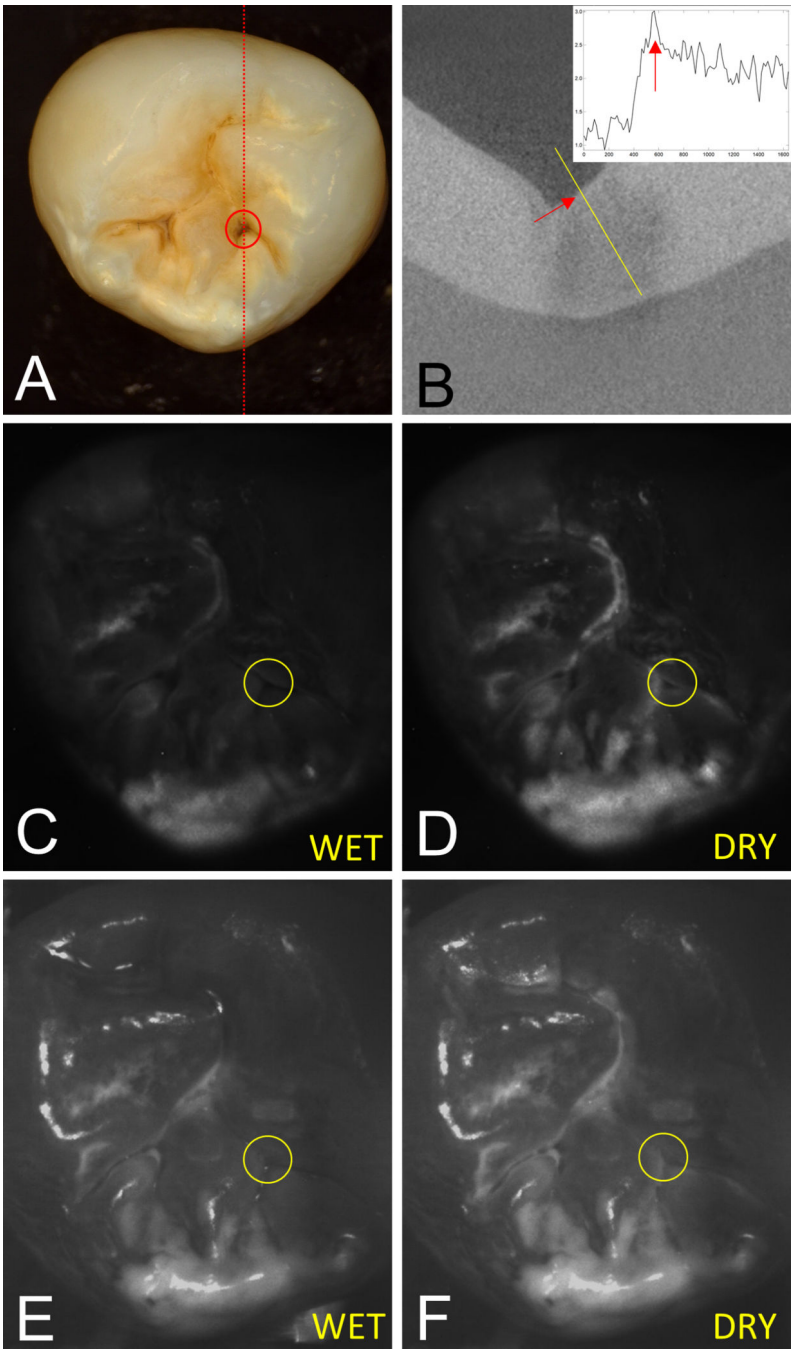


**Fig. 4.**

(A) Color image of a tooth with an arrested lesion (red circle). (B) MicroCT image showing the lesion and inset shows a line profile of the mineral density vs position extracted at the position of the yellow line. Red arrow shows the position of the lesion surface zone in the extracted line profile. SWIR images acquired with the (C&D) benchtop system and handpiece (E&F) before (wet) and after (dry) drying the lesion for seconds. Yellow circle is the lesion area.

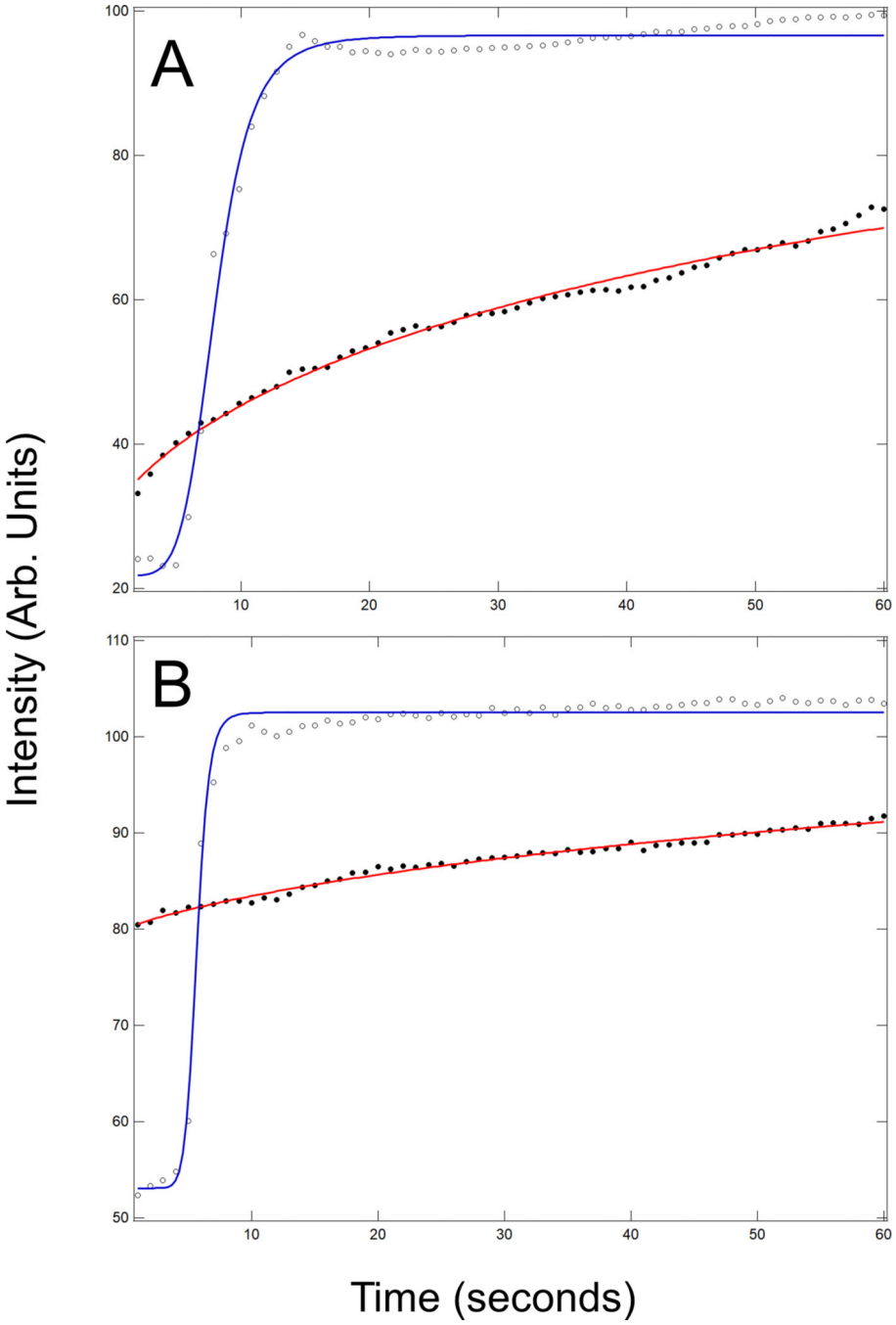


**Fig. 5.**

Plots of intensity vs time for the active (blue – open circles) and arrested (red – solid circle) lesions for (A) benchtop system and (B) handpiece. Solid red and blue lines are the fits using the Hill equation that were used to calculate the rates.

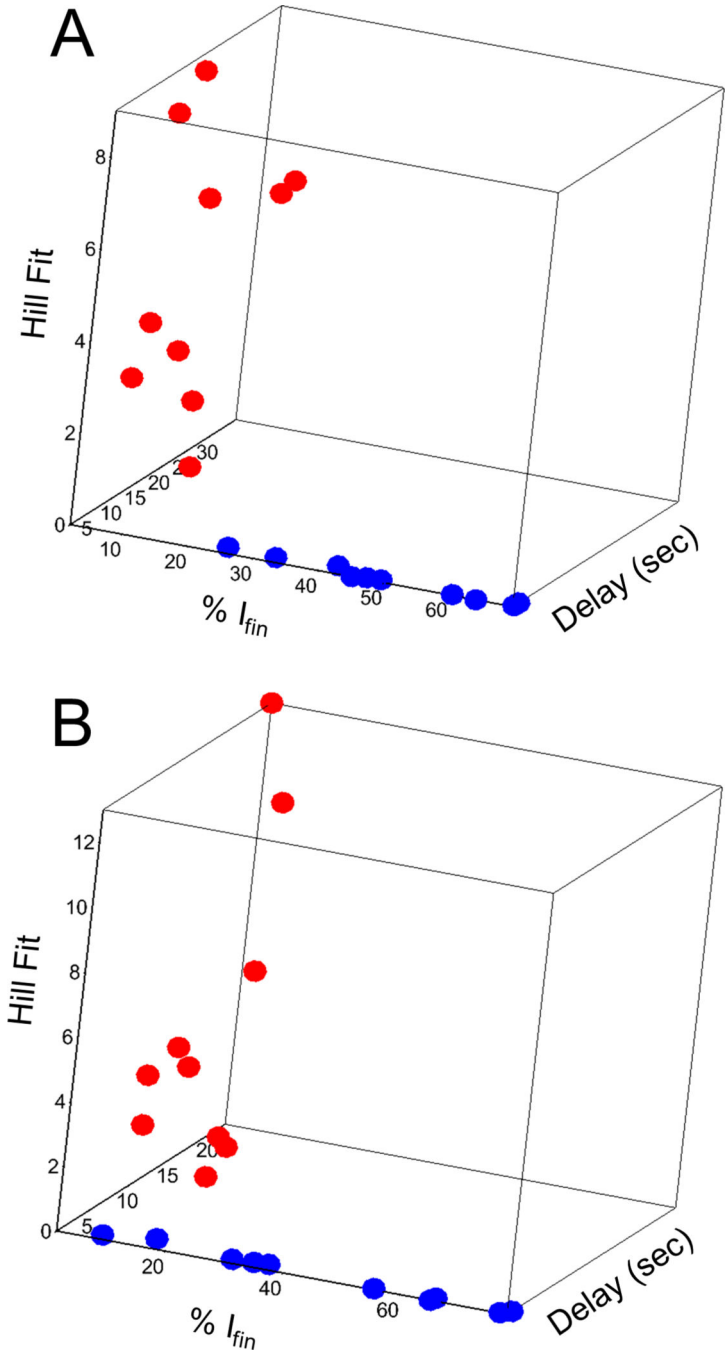


**Fig. 6.**

3D scatter plots of the DEL, % $I_{fin}$, and rate for the (A) benchtop system and the (B) handpiece. Red circles are active lesions and blue circles are arrested lesions.

**Table I.**

Mean ± sd of the Delay, %ΔI, $\%I_{fin}$, and rate (Hill) after 60 seconds of drying for the active (n=10) and arrested (n=10) lesion areas. Significance level is indicated for each t-test.

| **Benchtop** | **Delay** | **%ΔI** | $\%I_{fin}$ | **Rate (Hill)** |
|---|---|---|---|---|
| Active | 4.91±2.77 | 121±76.3 | 8.39±4.18 | 14.1±9.28 |
| Arrest | 0.00±0.00 | 145±253 | 50.4±15.0 | 1.03±1.72 |
| Significance | P<0.0001 | P<0.015 | P<0.0001 | P<0.0001 |
| **Handpiece** | | | | |
| Active | 5.4±3.95 | 51.4±35.6 | 13.0±8.93 | 9.13±6.16 |
| Arrest | 0.00±0.00 | 51.5±50.6 | 46.6±24.9 | 1.20±0.48 |
| Significance | P<0.0001 | P>0.40 | P<0.0033 | P<0.0001 |